Throughfall spatial patterns translate into spatial patterns of soil moisture dynamics – empirical evidence

Christine Fischer[1,2], Johanna Clara Metzger[1,3], Gökben Demir[1], Thomas Wutzler[4], Anke Hildebrandt[1,5]

[1]Institute of Geosciences, Friedrich-Schiller-University Jena, Burgweg 11, D-07749 Jena, Germany
5 [2]Office for Green Spaces and Waters, City of Leipzig, Prager Straße 118-136, D-04217 Leipzig, Germany
[3]Institute of Soil Science, University of Hamburg, Allende-Platz 2, 20146 Hamburg, Germany
[4] Max-Planck-Institute for Biogeochemistry, Jena, Germany
[5] Department Computational Hydrosystems, Helmholtz Centre for Environmental Research - UFZ, Leipzig, Germany

Correspondence to: Anke Hildebrandt (hildebra@alum.mit.edu)

10 **Abstract.** Throughfall heterogeneity induced by the redistribution of precipitation in vegetation canopies has repeatedly been hypothesized to affect the variation of soil water content and runoff behavior, especially in forests. However, observational study relating the spatial variation of soil water content directly to net precipitation are rare and few confirm modelling hypotheses. Here, we investigate whether throughfall patterns affect the spatial heterogeneity of soil water response in the main rooting zone. We assessed rainfall, throughfall and soil water contents (two depths: 7.5 cm and 27.5 cm) on a 1-ha
15 temperate mixed beech forest plot in Germany during the growing seasons 2015 - 2016 in independent high-resolution stratified random designs. Because throughfall and soil water content cannot be measured at the same location, we used kriging to derive the throughfall values at the locations where soil water content was measured. We first explore the spatial variation and temporal stability of throughfall and soil water patterns, and next evaluate the effects of input (throughfall), soil properties (field capacity and macroporosity), and vegetation parameters (canopy cover and distance to the next tree) on soil water content
20 and dynamics.

Throughfall spatial patterns were related to canopy density. Although spatial auto-correlation decreased with increasing event sizes, temporally stable throughfall patterns emerged, leading to reoccurring high and lower input locations across precipitation events. Linear mixed effect model analysis showed, that soil water content patterns were poorly related to spatial patterns of throughfall, and were more influenced by unidentified but time constant factors.

25 Instead of soil water content itself, the patterns of its increase after rainfall corresponded more closely to throughfall patterns, in that more water was stored in the soil where throughfall was elevated. Furthermore, soil moisture patterns themselves enhanced or decreased water storage in the soil, and probably fast drainage and runoff components. Locations with low topsoil water content tended to store less of the input water, indicating preferential flow. In contrast in subsoil, locations with high water content stored less water. Also, distance to the next tree and macroporosity modified how much water was retained in
30 soil storage. Overall, throughfall patterns imprinted less on soil water contents and more on soil water dynamics shortly after rainfall events, therefore percolation rather than soil water content may depend on small scale spatial heterogeneity of canopy input patterns.

1 Introduction

Over the past decades, there has been a raised interest on how water input at the soil surface is affected by vegetation
canopies to understand and predict hydrological processes related to vegetation structure and land use change (Guswa et al.,
2020; Murray, 2014; Oda et al., 2021; Savenije, 2004; Western et al., 2004). Due to interception losses, the water arriving
below the canopy is a smaller amount compared to above (Horton, 1919 and references therein; Carlyle-Moses and Gash,
2011) with implications for the soil water balance (Bouten et al., 1992; Durocher, 1990; Klos et al., 2014; Metzger et al.,
2017; Schume et al., 2003) and overall water budget at the catchment scale (Brown et al., 2005; Oda et al., 2021).

Besides interception loss, interaction of precipitation with the vegetation canopy causes spatial redistribution of the incoming
water. This leads to characteristic spatial heterogeneity of the dripping (throughfall) and flowing (stemflow) below canopy
precipitation, locally causing enhanced water input to the soil surface. For example, hotspots by dripping points (enhanced
water flow from peculiarities in the canopy, Falkengren-Grerup, 1989; Keim et al., 2005; Staelens et al., 2006; Voss et al.,
2016) and stemflow hotspots (Carlyle-Moses et al., 2018; Levia and Germer, 2015) are well-documented. The available
research suggests that both throughfall patterns and stemflow spatial distributions are reoccurring (Guswa and Spence, 2012;
Keim et al., 2005; Metzger et al., 2017; Staelens et al., 2006; Van Stan et al., 2020; Wullaert et al., 2009; Zimmermann et al.,
2008).

The observed persistence of spatial patterns of below canopy precipitation has created a strong expectation that those affect
patterns of soil water content (Rosenbaum et al., 2012; Schume et al., 2003; Wullaert et al., 2009; Zehe et al., 2010) and
hotspots of percolation or preferential flow (Bachmair et al., 2012; Blume et al., 2009; Bouten et al., 1992; Schume et al.,
2003) in forests soils. Yet, this is only partly confirmed with observations: For stemflow affected locations, soil moisture
microsites have repeatedly been demonstrated (Durocher, 1990; Germer, 2013; Liang et al., 2007; Metzger et al., 2021;
Pressland, 1976). Stemflow can create substantial funneling of water to the forest floor and water availability on the forest
floor can be locally enhanced 10 to 100 times (Carlyle-Moses et al., 2018; Levia and Germer, 2015; Metzger et al., 2021).

For stemflow is has been repeatedly conformed that hotspots of above ground water input has belowground consequences.
Much less research is available about on how the less pronounced, but still spatially persistent pattern of throughfall shapes
soil water dynamics. Modelling suggested that throughfall patterns influence the root zone soil moisture pattern (Coenders-
Gerrits et al., 2013; Guswa, 2012). However, soil moisture patterns are also influenced by several other factors creating
substantial heterogeneity such as heterogeneity of soil properties, local micro-topography, litter thickness or root water
uptake (Bouten et al., 1992; Gerrits and Savenije, 2011; Liang et al., 2017; Molina et al., 2019; Rosenbaum et al., 2012;
Schume et al., 2003; Schwärzel et al., 2009), and those are typically not fully captured in virtual experiments. In contrast,
observation studies found that throughfall and root zone soil moisture were not (Rodrigues et al., 2022; Shachnovich et al.,

2008) or only occasionally (Metzger et al., 2017) or weakly (Molina et al., 2019) related. On the other hand, Klos et al. (2014) found a relation below the rooting zone by strategically sampling at high and low throughfall positions, and several authors found indirect evidence by interpreting the change of spatial variation in soil water content (Metzger et al., 2017; Rosenbaum et al., 2012; Zehe et al., 2010) after precipitation events.

70

In light of the substantial heterogeneity of other influencing factors, one of the reasons for the limited direct observational evidence of the effect of throughfall on soil water content maybe the limited number of studies investigating the relation between below canopy precipitation and soil water patterns in a dedicated and coordinated fashion. The characterization of spatial patterns, such as those of throughfall, requires a large number of samplers (Kimmins, 1973; Lloyd and Marques,

75   1988; Van Stan et al., 2020; Zimmermann et al., 2010), and the same is true for below ground observations. Furthermore, a fundamental challenge is that soil water input and soil water content cannot be assessed at the same location, since the throughfall measurements disturb the infiltration into the soil. The objective of this study is therefore to compare the patterns of soil water content, soil properties and throughfall using a dedicated spatially highly resolved sampling design to reveal whether input, next tree distance or soil properties affect spatial variation in soil water content and soil water response. We

80   used independent designs for above and below ground observations and applied kriging to derive the throughfall values at the locations where soil water content was measured. The aims of the study were to a) to explore spatial heterogeneity and temporal stability of throughfall and soil water content and b) evaluate the influence of soil properties (field capacity and macroporosity), vegetation parameters (canopy cover, next tree distance) and input variation (throughfall) on the variation of soil water content and soil water content increase after precipitation.

85   **2 Methods**

2.1 Study area

The study was carried out in the Hainich Critical Zone Exploratory (CZE Hainich, see Küsel et al. 2016), run by the Collaborative Research Centre "AquaDiva". The site is located in Central Germany, in the Hainich National Park in an unmanaged beech dominated forest. Mean annual temperature is around 7.5 to 9.5 °C, depending on the position on the small

90   mountain range. The total annual precipitation drops from 900 to less than 600 mm from ridge to valley (Küsel et al., 2016). The monitoring site as well as measurements of precipitation and soil moisture have been described in Metzger et al. (2017), and the important parts are repeated here for completeness. The site covers an area of 1 ha and is situated at 365 m a.s.l.. The study area contains of 581 tree individuals (diameter breast height ≥ 5 cm), representing a heterogeneous age structure. The soils in this area are dominatly luvisols (Kohlhepp et al., 2017; Schrumpf et al., 2014). The species assemblages consists of

95   70% European beech trees (*Fagus sylvatica*), as well as Sycamore maple (*Acer pseudoplatanus*), European ash (*Fraxinus excelsior*), European hornbeam (*Carpinus betulus*), Large-leafed linden (*Tilia platyphyllos*), Norway maple (*Acer platanoides*) and Scots elm (*Ulmus glabra*). The weathered bedrock is at 15 to 87 cm depth (median depth 37 cm).

2.2 Precipitation measurements and processing

100 The precipitation sampling follows the same procedure as given in Metzger et al. (2017). Gross precipitation (P_g) and throughfall (P_{TF}) were measured manually on a per-event basis in spring 2014, 2015, 2016. The analysis for effects of throughfall on soil water content covers the period when also soil moisture sensors were active, that is from June 18 to July 28 2015 and May 31 to July 14 2016. The installed throughfall collectors consist of circular funnels (A = 0.011 m^2), the opening of which is placed about 37 cm above the ground surface. A table tennis ball is placed in the opening of the funnel to minimize

105 evaporation.

Throughfall collectors were arranged in a stratified sampling design (Zimmermann et al., 2016). For this, the 1 ha plot was divided into 100 subplots each 10 m x 10 m (Figure 1) and equipped with two randomly located throughfall samplers. Of those, we selected 50 points randomly and added another sampler in immediate vicinity (0.1 m distance) creating a "short transect". Furthermore, to 25 randomly selected short transects we added four more samplers at 0.5, 1, 2, and 3 m from the

110 first to form "long transects". The direction of all transects was also randomly chosen. In total we sampled n = 350 throughfall positions. Sampling started 2 h after the end of rainfall by collecting the volume of all sampling containers using graduated cylinders. Gross precipitation was measured at an adjacent (distance 250 m) open grassland using five funnels of the same type as the throughfall collectors.

In this research, we are specifically interested in re-occurring spatial patterns of throughfall and whether they translate to soil

115 water dynamics. To characterize the spatial pattern, we decompose the measured throughfall into spatial median ($\hat{P}_{TF,j}$) of event j and deviations from the median at the specific location i ($\delta P_{TF,ij}$). The latter are calculated as:

$$\delta P_{TF,ij} = \frac{P_{TF,ij} - \hat{P}_{TF,j}}{\hat{P}_{TF,j}} \tag{1}$$

where $\delta P_{TF,ij}$ represents the relative deviations of the spatially distributed throughfall ($P_{TF,ij}$) at locations i and event j from the spatial median $\hat{P}_{TF,j}$ of that event j. Eq 1 is a slight modification of the widely used concept of temporal stability introduced by Vachaud et al. (1985). Since throughfall can contain outliers, we used the median ($\hat{P}_{TF}$) instead of the arithmetic mean for

120 normalization, as already done by Zimmermann et al. (2008) and Wullert et al. (2009) Negative (positive) values of $\delta P_{TF,ij}$ indicate locations with below (above) average throughfall, while repeatedly low (high) $\delta P_{TF,ij}$ indicate persistent cold (hot) spots of canopy throughfall across events. Eq. 1 allows disentangling the temporal variation, e.g. the event size given by the event spatial median $\hat{P}_{TF,j}$, from the spatial dispersion, characterized by $\delta P_{TF,ij}$. Both are independent of each other and both are used in parallel as predictors for soil water content and soil water content increase below. In the following we drop indices

125 i and j for simplicity and refer to δP_{TF} as the spatial pattern of throughfall for an event or event class.

To investigate the temporal persistence of the spatial pattern of throughfall we derived temporal stability plots (Wullaert et al., 2009; Zimmermann et al., 2008) by looking at $\delta P_{TF,ij}$ across events at the specific location i. Additionally, we calculated

Spearman rank correlation coefficients between observations of different events, where high correlations indicate strong persistence (or temporal stability) of the throughfall pattern. We paired all events falling into a given rain event class according to Metzger et al. (2017): small: ($P_g \leq 3$ mm); medium (3 mm $< P_g \leq 10$ mm), large ($P_g > 10$ mm).

To relate the general precipitation and soil moisture conditions during the observation period to the average climate, we compared them with precipitation data from a nearby gauge (Mühlhausen- Windeberg, 20 km to the northeast) of the German Weather Service (DWD climate data centre, www.dwd.de/cdc, ID 5593).
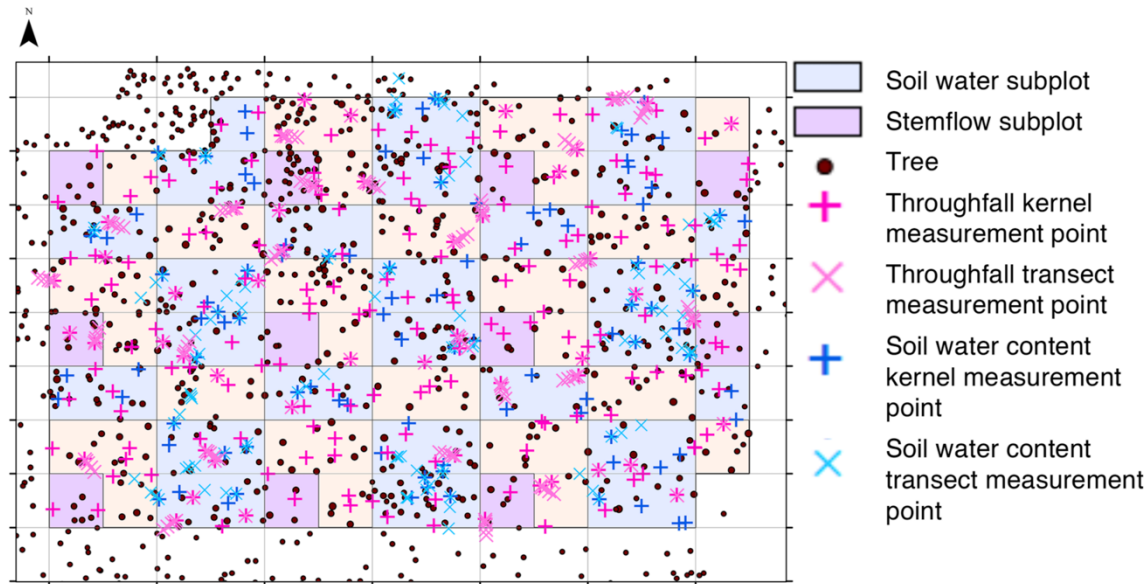
Fig. 1: Experimental set-up in the 1-ha forest plot subdivided by a 10 m x 10 m grid yielding 100 subplots. Positions of the throughfall samplers (pink crosses) and 49 soil water content subplots (blue) measured in a stratified random design with transects (see material and methods for more details, Figure from Metzger et al., 2017).

2.3 Soil water content measurements

The soil water measurements were first described in Metzger et al. (2017). Volumetric soil water content was monitored using a wireless sensor network (SoilNet, Bogena et al. (2010)) equipped with SMT100 frequency domain sensors (Truebner GmbH, Neustadt, Germany). Overall 210 soil water content measurement points were distributed in a stratified random design in the blue subplots shown in Figure 1: Within each blue subplot, two sampling points were placed randomly. Additionally, to a subset of 24 randomly selected points, transects were added with three additional measurement points (at 0.1, 2.0, and 6.0 m from the position). Furthermore, 40 locations were added as transects near tree stems. At each soil moisture measurement

location, sensors were installed in two depth, e.g topsoil 7.5 cm and subsoil 27.5 cm depths. For this analysis we used the data collected during the throughfall measurement campaigns from June 18 to July 28 2015 and May 31 to July 14 2016.

At each location, we used soil moisture measurements an hour preceding the observed rain event ($\theta_{\text{pre,ij}}$) to characterize soil initial moisture in the drained state and the maximum soil water content just after the rain event ($\theta_{\text{post,ij}}$) to characterize the post event state. We also assessed the soil water content increase due to rainfall by calculating the change of soil water content ($\Delta\theta_{ij}$) for each event j and each location i with

$$\Delta\theta_{ij} = \theta_{post,ij} - \theta_{pre,ij} \tag{2}$$

positive values of $\Delta\theta_{ij}$ indicate soil water content increase. In the following, we refer generally to $\Delta\theta$ (with indices dropped for simplicity) as "soil water content increase" or "soil moisture response" due to rainfall.

Equivalently to throughfall, we decomposed soil water content into the event spatial median ($\hat{\theta}_{\text{pre,j}}$, $\hat{\theta}_{\text{post,j}}$) and relative deviations from that median ($\delta\theta_{\text{pre,ij}}$, $\delta\theta_{\text{post,ij}}$) with indices for event j and location i dropped for simplicity in the following. As for throughfall, using the relative deviations of soil water content alongside the medians in the statistical models (see below) provides us with two independent measures for one variable, one relating to spatial pattern ($\delta\theta_{\text{pre,ij}}$, $\delta\theta_{\text{post,ij}}$) and the other to temporal variation ($\hat{\theta}_{\text{pre,j}}$, $\hat{\theta}_{\text{post,j}}$).

2.4 Canopy and soil property measurements

At the time of soil sensor installation, undisturbed soil samples were collected using metal ring cylinders with a volume of 100 cm^3. The distance between the sensor position and the soil sample collection was approximately 0.5 m. Soil properties were treated as if they were measured directly at the soil sensor location i. In order to determine field capacity ($\theta_{\text{FC,i}}$), the samples were first saturated and next let drain in a sand box with a hanging water column imposing a pressure of −60 hPa for 72 hours and weighed. The soil cores were subsequently dried for 24 h at 105° C and weighed again to obtain the dry weight $m_{\text{dry,i}}$. The volumetric water content at field capacity ($\theta_{\text{FC,i}}$) was derived from the weight difference of the sample at -60 hPa and the dried one, while assuming a density of water of $D_{\text{w}} = 1$ g cm^{-3}. Bulk density ($D_{\text{bd,i}}$) was calculated from soil dry weight and volume. Soil apparent porosity (φ_i) was calculated from the bulk density and assuming a constant density of the soil mineral component ($D_{\text{m}} = 2.66$ g cm^{-3})

$$\varphi_i = 1 - \frac{D_{bd,i}}{D_m} \tag{3}$$

Macroporosity ($\theta_{\text{MP,i}}$, also called air capacity or air-filled porosity) was then determined as

$$\theta_{MP,i} = 1 - \theta_{FC,i} \tag{4}$$

To characterize the canopy density, we counted the number of branches (canopy cover) above the throughfall samplers in 2014. This data was however not available for soil water measurement locations.

2.5 Statistical Analysis

175 All statistical analysis were processed with R 3.2.3 (Core Team 2016). For the geostatistical analysis (detailed below) we used the the packages *geoR* (Ribeiro Jr and Diggle, 2001), *georob* (Papritz and Schwierz, 2020) and *gstat* (Gräler et al., 2016; Pebesma, 2004). Linear mixed effects models were implemented using the package *lme4* (Bates et al., 2015) and *lmerTest* (Kuznetsova et al., 2017). The variance explained by fixed and random factors (conditional R²) and by only fixed effects (marginal R², Nakagawa and Schielzeth (2013)) for the final model were calculated with the *MuMIn* package (Barton, 2020).

180

2.5.1 Geostatistical estimation of throughfall

Throughfall was estimated at the soil water content measurement locations by kriging. The overall procedure for obtaining the variograms closely follows Zimmermann et al. (2016) with some adaptations taken from Voss et al. (2016). Important steps and decisions of the exploratory data and geostatistical analysis are shown in Figure S1.

185

1. Exploratory Analysis-Test for trends and underlying asymmetry. First, we determined the skewness using the octile skew. The octile skew of none of the throughfall events was larger than 0.2 or smaller than -0.2 and we therefore did not transform the data. If a spatial trend existed ($p \leq 0.150$), we used the residuals of the spatial regression model for the coordinates x and/or y instead of the real data in the following.

190

2. Variogram estimation by the method-of-moments (MoM). This step was performed to derive the best possible preliminary variogram with outliers present, which will be used for spatial outlier detection in step 3. For this, we first calculated four empirical throughfall variograms using four different variogram estimators. We used both non-robust (Matheron, 1962) and robust (Cressie and Hawkins, 1980; Dowd, 1984; Genton, 1998) estimators and the *sample.variogram* function in the package 195 *georob* in R. We chose lags centered at 0.125, 0.375 and 0.75, followed by a step size of 1 m up to 50 m). Next, we fitted to each empirical variogram three models (spherical, exponential and pure nugget) using *fit.variogram.model* function in the package *gstat* and chose for each the model with the lowest Residual Sum of Squares. This yielded four models, one for each of the variogram estimators stated above. Then we assessed the fitted models by leave-one-out cross validation using kriging. Based on this we calculated the normalized kriging error (Θ_i,) and selected for step 3 the empirical variogram with median Θ 200 nearest to the expected value of 0.455 (Lark, 2000) as done in Zimmermann et al. (2009)

3. Identification and spatial outlier removal. Before final variogram estimation using residual maximum likelihood (REML) in step 4, spatial outliers were removed based on kriging and cross validation using the provisional variagram obtained in step 2. For identifying a spatial outlier at location *i* we used the standardized error of cross validation $\varepsilon_{s,i}$ (Bárdossy and Kundzewicz,

1990, Lark, 2002). To classify an outlier we used the Z-statistics. Sampled points with $\varepsilon_{s,i} < -2.576$ ($\alpha/2 = 0.005$) were removed (Zimmermann et al., 2016).

4. Variogram estimation by residual maximum likelihood (REML). After outlier removal, we applied REML to fit the theoretical variogram model including spatial trend if necessary, using the *likfit* function in the package *geoR*. We used the initial estimates from the provisional variogram (step 2) for the parameters sill, nugget and range. The range relates to the distance over which the observations are still spatially correlated. In the following, we will use the term correlation length to refer to the effective range, e.g. the distance at which the variogram approaches the sill to 95%. A high effective range indicates a high spatial correlation between two throughfall collectors. We checked the reliability of the final model with the statistic Θ_i (see above).

5. Kriging. Using the final theoretical variogram from step 4, we applied ordinary kriging to predict throughfall values at the soil water content measurement locations. Locations where the kriging variance exceeded 95% of the spatial variance were removed from further analysis.

2.5.2 The coefficient of quartile variation (CQV)

For event scale assessments, we used quantile based statistical metrics for descriptive statistics and correlation, to avoid bias related to event size or general soil moisture state. Both throughfall and soil moisture patterns can be skewed (Famiglietti et al., 1998; Zimmermann and Zimmermann, 2014) slightly even if the octile skew is less than 0.2 depending on soil moisture state or event size. Also, as mentioned above, throughfall typically includes outliers due to dripping points (Falkengren-Grerup, 1989; Keim et al., 2005; Staelens et al., 2006; Voss et al., 2016). For the coefficient of variation, we used the quartile variation coefficient (CQV) (Bonett, 2006) as alternative to the coefficient of variation:

$$CQV = \frac{Q3 - Q1}{Q3 + Q1}$$

where Q1 and Q3 represent first and third quartiles. Like the classical coefficient of variation, the CQV is dimensionless statistical measure that describes the relative degree of scattering of the sample.

2.5.3 Linear mixed effects models calculation

We applied linear mixed effect models (LME) with repeat-measurement structure to evaluate the influence of potential drivers explaining soil water content or soil water content increase. We present results on the following dependent variables (see Table 1 for an overview): Spatial pattern of pre-event ($\delta\theta_{pre}$), and post-event ($\delta\theta_{post}$) soil water content as well as soil water content increase ($\Delta\theta = \delta\theta_{post} - \delta\theta_{pre}$).

235 The independent variables (fixed effects) for $\delta\theta_{pre}$ were: Gross precipitation (P_g), nearest tree distance (d_{tree}), macroporosity (θ_{MP}), field capacity (θ_{FC}), throughfall of the preceding event ($P_{TF,prec}$). The independent variables (fixed effects) for $\Delta\theta$ and $\delta\theta_{post}$ were: Gross precipitation (P_g), spatial median of soil pre-event water content ($\hat{\theta}_{pre}$), spatial pattern of soil pre-event water content ($\delta\theta_{pre}$), nearest tree distance (d_{tree}), macroporosity (θ_{MP}), field capacity (θ_{FC}), spatial median of throughfall ($\hat{P}_{TF}$) and spatial pattern of throughfall (δP_{TF}). Year, day of year and sensor position were implemented as random effects accounting

240 for repeated measurements. To avoid model over-fitting it is important that there are no strong correlations between the explanatory variables (Graham, 2003). To detect multi-collinearity and to avoid potentially spurious models we calculated Spearman rank correlation coefficients (ρ) for all pairs of predictors (Table S1). Before the analysis we removed one of a pair of highly correlated predictors: Gross precipitation (P_g, strong correlation with $\hat{P}_{TF}$) and field capacity (θ_{FC}, strong correlation with θ_{MP}). All variables (predictor and response) were scaled to center around zero and have a standard deviation of one (z-

245 transformation). In this way, the fitted slopes of the model indicate how strongly a change of the predictor within its own range affects the response variable within its own range and hence the slope estimate gives insight into the effect strength. Scaling has no effect on model selection. To obtain the minimal adequate models for the response variables, we started with the maximum model and removed stepwise all non-significant terms based on the Akaike Information Criterion (AIC). Main effects included in significant interactions were retained in the model.

250 **Table 1: Overview of variables and symbols used in the statistical models.**

Symbol	Description	Applies to
Variables		
P_g	Event gross precipitation (mm)	
P_{TF}	Event throughfall (mm)	
θ	Volumetric soil water content(vol-%)	
θ_{FC}	Field capacity (vol-%)	
θ_{MP}	Macroporisity (vol-%), Eq. 4	
Indices		
i	Location	All
j	Event	All except θ_{FC}, θ_{MP}
prec	Preceding event	$P_{TF,prec}$
pre	Assessed before start of the event	$\hat{\theta}_{pre}$, $\delta\theta_{pre}$
post	Assessed after the end of the event	$\hat{\theta}_{post}$, $\delta\theta_{post}$
Operations		
$\hat{X}_j$	Spatial median of variable X, evaluated at given event j. The index j is dropped for simplicity.	$\hat{\theta}_{pre}$, $\hat{\theta}_{post}$, $\hat{P}_{TF}$
δX_{ij}	Deviation of variable X from the spatial median, assessed at each location i and event j, see Eq.1. The ensemble of δX for a given event makes up the "spatial pattern". Indices are dropped for simplicity.	$\delta\theta_{pre}$, $\delta\theta_{post}$, δP_{TF}
$\Delta\theta_{ij}$	Temporal change of soil water content, also referred to as "soil moisture increase" due to rainfall or "soil moisture response", with units of vol-%. See Eq. 2. Indices are dropped for simplicity.	$\Delta\theta_{ij} = \theta_{post,ij} - \theta_{pre,ij}$

Table 2: Overview of observed rainfall event properties. Event date, gross precipitation (P_g), spatial statistics of throughfall (P_{TF}), soil water content before (θ_{pre}) and after (θ_{post}) the rain event, as well as the soil water content increase ($\Delta\theta$) in topsoil and subsoil: spatial median (med), coefficient of quartile variation (CQV), interquartile range (IQR), and effective range (Range).

			Precipitation				Topsoil water content						Subsoil water content					
Date	P_G	Event			P_{TF}		θ_{pre}		θ_{post}		$\Delta\theta$		θ_{pre}		θ_{post}		$\Delta\theta$	
		size	med	CQV	IQR	Range	med	CQV	med	CQV	med	CQV	med	CQV	med	CQV	med	CQV
	mm		mm	-	mm	m	Vol-%	-	Vol-%		Vol-%	-	Vol-%	-	Vol-%	-	Vol-%	-
21.07.2015	1.6	small	0.6	0.29	0.4	9.6	21	0.16	21	0.17	0.08	2.6	36	0.10	36	0.10	-0.04	-3.34
20.06.2015	2.1	small	0.4	0.60	0.5	9.8	19	0.15	19	0.15	0.00	5.0	30	0.13	30	0.13	0.30	0.27
30.05.2015	2.8	small	1.7	0.21	0.7	9.2	27	0.14	27	0.14	0.03	1.0	37	0.11	37	0.11	0.00	-1.00
18.06.2015	3.3	medium	1.8	0.28	1.0	5.8	19	0.15	20	0.16	0.03	1.0	31	0.13	31	0.13	0.00	-1.47
13.07.2015	3.3	medium	1.9	0.22	0.8	8.6	17	0.14	17	0.14	-0.02	41.0	27	0.14	27	0.15	-0.01	-
02.06.2015	3.7	medium	1.8	0.25	0.9	8.0	26	0.14	26	0.14	0.00	3.0	37	0.12	37	0.12	0.00	-
13.05.2015	4.1	medium	2.7	0.19	1.0	7.6	34	0.11	35	0.10	0.71	0.89	41	0.08	41	0.08	-0.01	-1.00
11.07.2015	4.6	medium	2.7	0.13	0.7	8.9	17	0.14	18	0.13	0.13	1.00	27	0.14	28	0.14	0.72	0.32
25.07.2015	5.7	medium	3.9	0.14	11	4.6	19	0.13	21	0.14	0.41	0.98	33	0.11	33	0.11	0.00	-3.00
15.07.2015	10.5	large	6.6	0.18	2.4	5.9	17	0.14	19	0.17	1.5	0.76	27	0.14	28	0.14	0.33	0.65
08.07.2015	13.3	large	9.4	0.08	1.50	4.8	17	0.14	19	0.15	2.0	0.78	28	0.13	29	0.13	0.28	0.87
28.07.2015	20.1	large	13.7	0.16	4.4	7.5	19	0.13	23	0.21	4.1	0.57	32	0.12	35	0.12	2.60	0.71
24.06.2015	23.0	large	14.2	0.15	4.4	7.0	19	0.15	24	0.21	5.2	0.66	30	0.13	31	0.13	0.27	0.86
20.07.2015	35.2	large	29.2	0.06	3.5	5.9	16	0.15	22	0.19	6.4	0.56	27	0.14	33	0.14	5.43	0.65
28.06.2016	5.3	medium	2.6	0.25	1.3	7.8	26	0.13	25	0.14	0.00	-1.00	35	0.11	35	0.11	0.00	-1.00
21.06.2016	13.7	large	10.1	0.13	2.6	8.9	34	0.10	38	0.09	3.90	0.23	39	0.09	42	0.09	1.56	0.53
06.06.2016	16.9	large	14.9	0.09	2.8	3.0	34	0.09	39	0.09	4.33	0.31	41	0.09	43	0.08	1.58	0.43
02.08.2016	19.6	large	13.7	0.11	3.1	5.7	20	0.13	22	0.19	2.17	0.81	30	0.13	31	0.13	0.12	0.99
04.07.2016	19.8	large	11.9	0.14	3.4	9.5	23	0.14	25	0.16	1.60	0.83	32	0.11	33	0.11	0.01	1.51
25.05.2016	20.8	large	13.3	0.11	3.1	6.5	26	0.12	33	0.15	5.77	0.50	37	0.11	39	0.11	0.74	0.96
16.06.2016	23.2	large	15.2	0.11	3.3	7.3	35	0.12	37	0.10	2.21	0.27	40	0.09	40	0.09	0.01	5.84
14.07.2016	24.1	large	20.0	0.10	4.0	5.0	21	0.17	22	0.20	0.99	0.89	39	0.09	42	0.09	2.81	0.50
31.05.2016	25.0	large	21.0	0.11	4.4	4.6	30	0.12	39	0.09	8.05	0.21	39	0.09	43	0.09	3.98	0.38
25.07.2016	33.5	large	25.6	0.13	6.6	3.5	22	0.15	23	0.18	0.42	0.96	33	0.13	35	0.13	1.34	0.48
	2.2	small	0.9	0.4	0.54	9.5	22	0.15	23	0.15	0.04	2.87	34	0.11	35	0.11	0.09	-1.36
	4.3	medium	2.5	0.2	0.95	7.3	23	0.15	23	0.15	0.2	6.67	33	0.11	33	0.11	0.11	-1.23
	20.3	large	14.8	0.1	3.54	5.6	23	0.13	27	0.15	3.27	0.62	34	0.11	36	0.11	1.40	0.82

3 Results

3.1 Precipitation, throughfall and soil water content pattern

The summer rainfall (May to October) for the last 30 years (1986 – 2016) shows an average of 352 mm (Mühlhausen-Windeberg). During the two summer periods of this study (2015 and 2016), the annual rainfall was below the long-term mean (276 and 303 mm, respectively). However, the summer 2015 were the third driest of the last 30 years (Metzger et al., 2017). The final winter months of 2014 were the driest and the hydrological year 2014/2015 the second driest of the 30 years period. The hydrological year 2015/2016 and the final winter months of 2015 received average precipitation.

Descriptive statistics of throughfall and soil water content (topsoil and subsoil) are given in Table 2. We observed 14 rainfall events in 2015 and ten in 2016. The gross precipitation ranged between 1.6 and 35.2 mm, with three small, six medium and five large in 2015, and one medium and nine large events in 2016. For both years, soil water content increased with soil depth (Table 2). The soil water content increase (difference between post-event and pre-event soil water content; $\Delta\theta$) was always higher in the topsoil compared to the subsoil. For smaller rainfall events, an increase in soil water content was mainly limited to the topsoil, and only following larger rainfall event, in both soil depths.

3.2 Spatial pattern of throughfall and soil water content

The relation between event size and correlation length of throughfall is shown in Figure 2. More detailed information about the spatial distributions and the variogram parameters is given in the supplement in Tables S2 and S3. Throughfall correlation lengths decreased with increasing event size from on average 6.2 m for large events to 7.5 m for medium and 9.5 m for small events. In comparison, canopy density correlation length was 7.5 m, i.e. similar to medium events. Throughfall and canopy density had a small nugget and a strong spatial dependence (nugget/sill ratio < 25%) for all events (Table S3). For both years, throughfall decreased significantly with increasing canopy density (Table S4), although most of the spatial variance of throughfall was related to unknown random effects. While canopy density had no spatial trend (Table S2), throughfall had a spatial trend in somewhat less than half of the events (Table S2). Those changed direction with time, were of varying strength and occurred in small as well as in large events.

The spatial variation of throughfall (inter-quartile range) increased with event throughfall, but the coefficient of quartile variation (CQV), which normalizes by event size, decreased (Table 2). The high Spearman rank correlation coefficient indicates a strong similarity of the spatial distribution of throughfall between individual events of the same size class (Figure 3). Thus, throughfall produced persistent wet and dry spots, also confirmed by time stability plots (Figure S2).

Soil water content spatial variation coefficients (CQV) decreased with increasing soil water content (expressed as the spatial mean) and consequently with increasing soil depth (Table 2, Figure S3). In the topsoil, the highest variation occurs in post-event soil water content (Figure S3) and is substantially higher compared to pre-event soil water content, indicating that the event response enhanced soil water content variation especially in moderately dry (summer) conditions in topsoil. However, the by far highest CQV were observed for the increase in soil water content after rain ($\Delta\theta$).
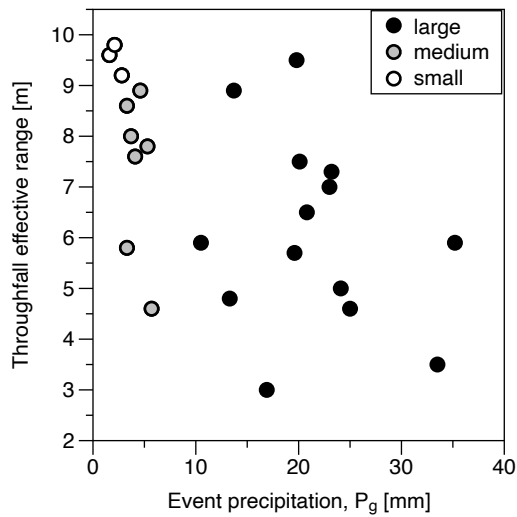
Fig. 2: Correlation length, given as effective range, derived from the throughfall variogram calculated for small ($P_g <$ 3 mm), medium (3 mm $< P_g <$ 10 mm), large ($P_g >$ 10 mm) events.
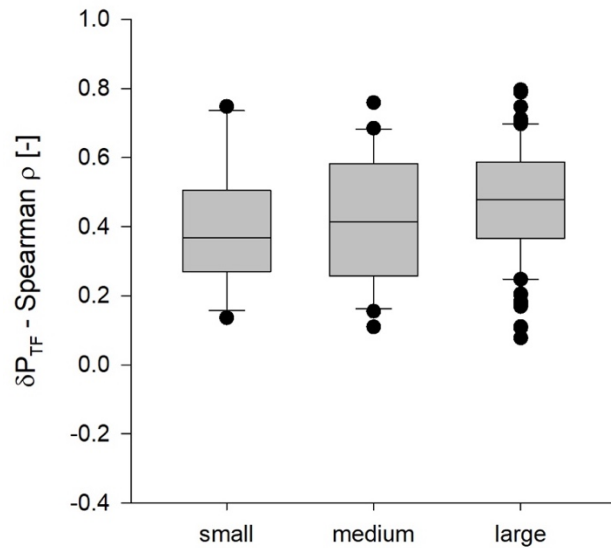
Fig. 3: Temporal stability of the spatial throughfall patterns. Shown are the pairwise correlation coefficients (Spearman) between throughfall (normalized deviation from the plot median (δP_{TF})) from different precipitation events, grouped by event size class (small (n=8), medium (n=11), large (n=21) events.
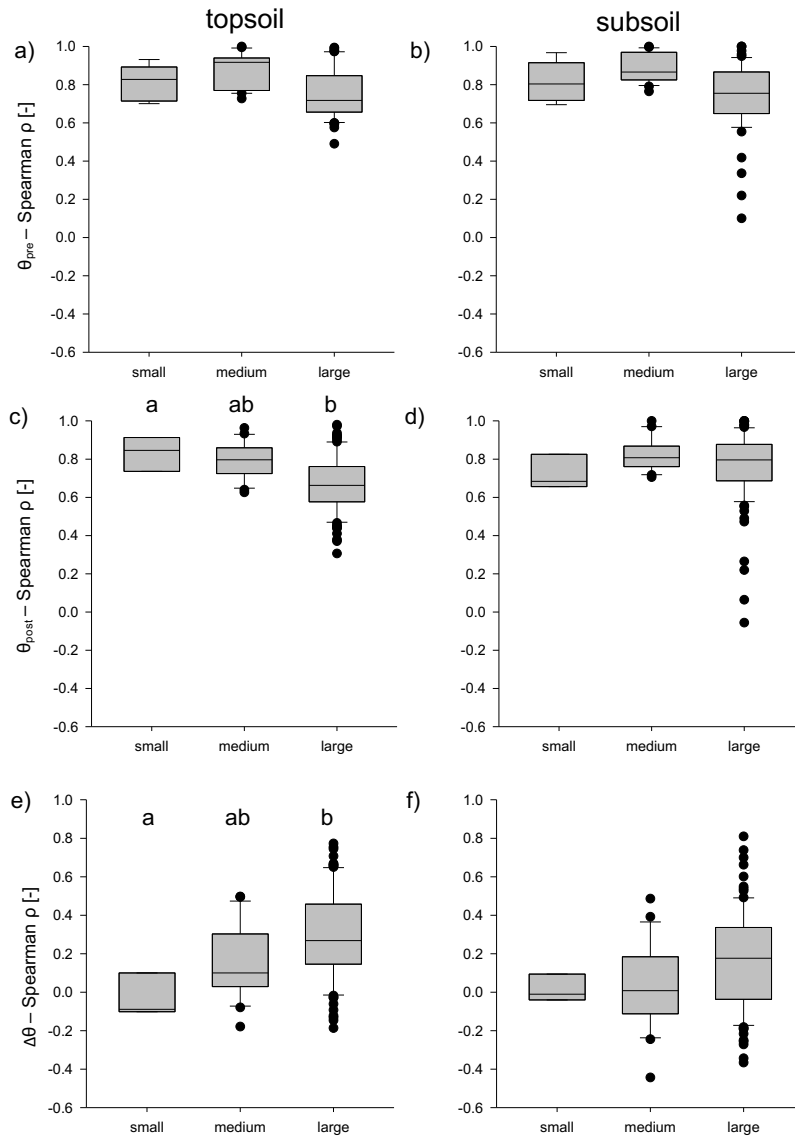
Fig. 4: **Temporal autocorrelation of spatial patterns of pre- and post-event soil water content and increase of soil water content after rainfall calculated as pairwise correlation coefficients (Spearman ρ) between all of the different precipitation events within the event size class (small (n = 3), medium (n = 7), large (n = 13). (top) pre-event soil water content (θ_{pre}); (middle) post-event soil water content (θ_{post}); (bottom) increase of soil water content ($\Delta\theta_i = \theta_{post} - \theta_{pre}$); (left) topsoil (-7.5 cm); (right) subsoil (-27 cm). The differences between the event size classes were examined using the Duncan's multiple range test. Letters on above the bars indicate significant difference (p ≤ 0.05) between the groups.**

The pairwise correlation coefficients indicating the temporal stability of the spatial patterns were high for pre-event (drained) soil water content (θ_{pre}) both in topsoil (Figure 4a) and subsoil (Figure 4b) with $\rho \approx 0.78$. For post-event soil water content (θ_{post}) they were significantly lower in the topsoil ($\rho = 0.70$, Figure 4c) than subsoil ($\rho = 0.77$, Figure 4d) (Mann-Whitney-U Test: $Z = -3.15$, $p = 0.002$). In the topsoil they decreased with increasing event size, revealing patterns were less similar after large precipitation events (Figure 4a,c). In contrast, spatial distribution in soil water content increase after rain events ($\Delta\theta = \theta_{post} - \theta_{pre}$) changed much more between events (Figure 4e,f), leading to an overall lower correlation between the patterns. However, the similarity of the spatial distribution of $\Delta\theta$ increased with event size especially in topsoil (Figure 4e), confirming reoccurring wetting patterns especially following larger events.

3.3 Factors influencing soil water spatial distribution

3.3.1 Soil water content

In order to identify the basic drivers for the patterns of soil water content in the drained state ($\delta\theta_{pre}$), we used mixed effects model selection. The resulting best models for top- and subsoil are given in Table 3. The variance explained by fixed effects (marginal R^2) was low, whereas the variance explained by fixed and random effects together (conditional R^2) was high. The model for the subsoil showed an even higher marginal R^2 compared to the topsoil, and a somewhat higher influence of fixed effects. The most important effect identified for topsoil and subsoil was macroporosity, with lower soil water content ($\delta\theta_{pre}$) related to locations of higher macroporosity (Table 3). In the topsoil also the throughfall of the preceding precipitation event slightly affected the soil moisture pattern. The results for the soil water content itself in the drained state (θ_{pre}) are similar to those of $\delta\theta_{pre}$, except that fixed effects explain even less variation.

Table 3: Factors affecting pre-event soil water content patterns ($\delta\theta_{pre}$) in topsoil and subsoil. Results for the best linear mixed effects model. Significant effects are highlighted in bold.

	topsoil		subsoil	
Explained variation				
R² Full model	0.818		0.822	
R² Fixed	0.035		0.143	
R² Random	0.783		0.679	
	slope	p-value	slope	p-value
Fixed effects				
Macroporosity, θ_{MP}	-0.181	**0.013**	-0.332	**<0.001**
Throughfall of preceding event, $P_{TF, prec}$	0.048	**0.039**	-0.030	0.144
Tree distance, d_{tree}	-0.063	0.426		
Interactions				
$P_{TF,prev}$ x θ_{MP}	-	-	-0.028	**0.007**
$P_{TF, prev}$ x d_{tree}	-0.021	**0.047**	-	-

The results of the best linear mixed effects model relating soil water content after a precipitation event to potential drivers is given in the Figure 5 (left panels) for all events and large events only (events with $P_g > 6$ mm). The median initial soil water content (soil water content before the rain event, θ_{pre}) and its spatial pattern ($\delta\theta_{pre}$) were the major drivers on either absolute

330 values of spatially distributed soil water content after the rain event (θ_{post}, Figure 5a,b) or its spatial pattern ($\delta\theta_{post}$). Other fixed ($\hat{P}_{TF}, \delta P_{TF}, \hat{\theta}_{pre}, \theta_{MP}, d_{tree}$) and random effects contributed only little, especially when small and medium events were excluded (Figure 5b).
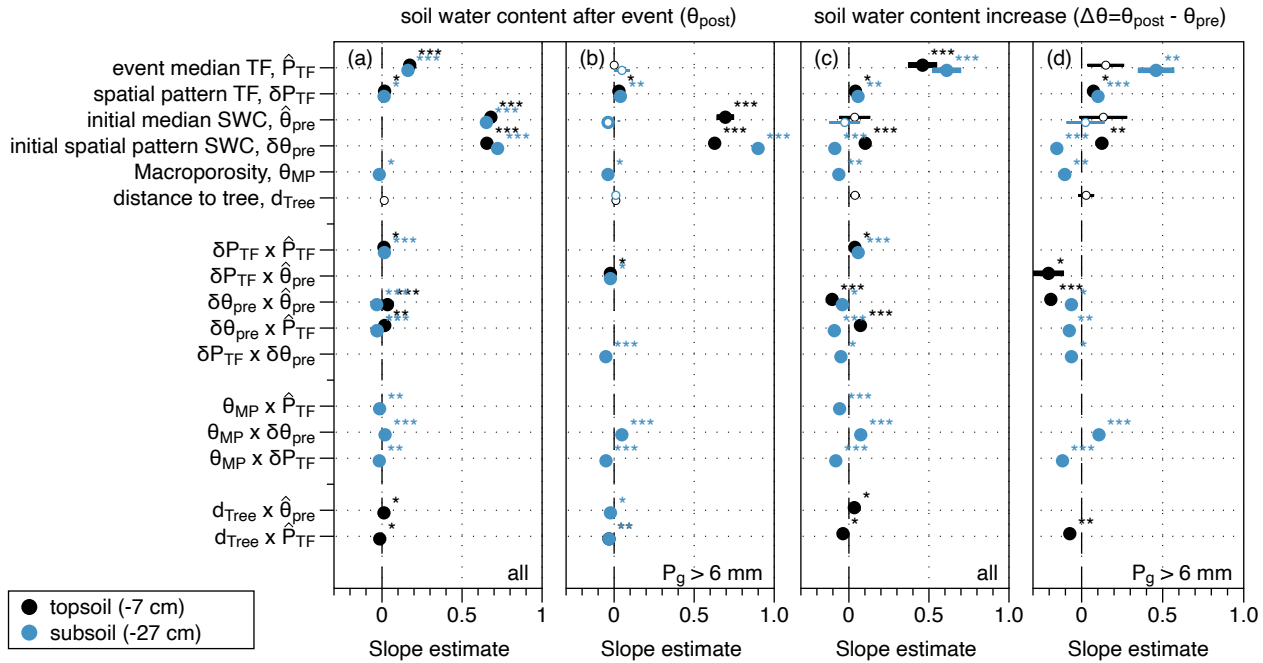
Fig. 5: Factors influencing (a, b) local post-event soil water content (peak soil water content after rainfall, θ_{post}) and (c,

335 d) local soil water content increase due to rainfall ($\Delta\theta$, difference between soil water content after and before each event). Slope estimates for the best linear mixed effects model including (a, c) all events, (b, d) large events only ($P_g > 6$ mm). Significant effects are shown with thick lines. Stars indicate level of significance (*** $p<0.001$, ** $0.001 \leq p<0.01$, * $0.01 \leq p<0.05$). All variables (predictors and responses) are z-scaled such that the slope indicates the effect strength. Pseudo R^2 values, summary of all models including those of small and medium events are given in the supplement

340 (Tables S5, S6).

3.3.2 Soil water response ($\Delta\theta$)

The slope estimates of models explaining the soil water content increase ($\Delta\theta$), i.e. how much water was locally added to the soil after rain, are visualized in Figures 5c and 5d for all and large events. In general, a detectable (> 1%) change of $\Delta\theta$ was

345   limited to large rainfall events (Table 2). The spatial patterns responded to several drivers (fixed effects) in the final model.
There, the variance explained by fixed effects (marginal R^2) was generally higher for subsoil compared to topsoil, it typically
increased with event size and was highest for the models including all event sizes (Table S6). In the following we therefore
focus on the effects emerging from models including all events. We also visualize models for events falling in the large event
class, as it covers more than 80% of the cumulated net precipitation received. The results for the individual event size classes

350   are given in the supplement (Tables S5 and S6).
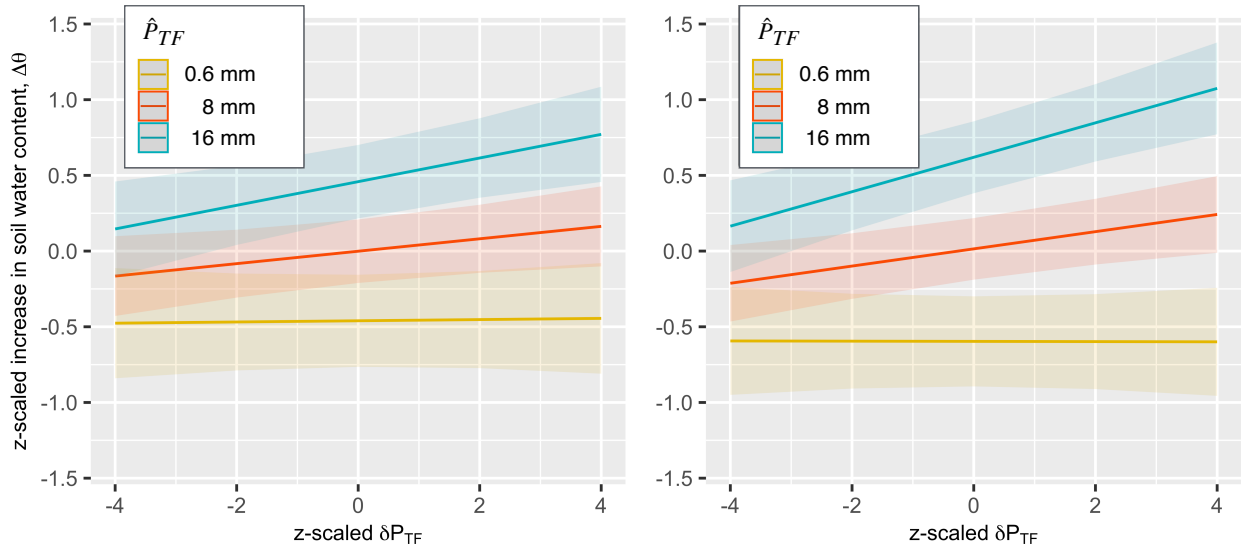
**Fig. 6: Marginal plot of the interaction between throughfall pattern (deviation of thoughfall from the spatial median)
and median event throughfall (δP_{TF} x $\hat{P}_{TF}$) affecting soil water content increase ($\Delta\theta$) for all events in topsoil (left) and
subsoil (right). Shown is the influence of the throughfall pattern (δP_{TF}) on the local soil water content response ($\Delta\theta_i$),**
355   **grouped by the event size (median event throughfall, $\hat{P}_{TF}$). Note that all values are z-scaled, such that the slope indicates
the effect strength. For example, the yellow line highlights small events, where the local soil water moisture response
depends little on spatial distribution of throughfall input. For large events, marked in blue, the soil moisture response
is stronger in locations of above average throughfall.**

360   Overall, local soil water content increase ($\Delta\theta_i$) depended not only on event median throughfall ($\hat{P}_{TF}$), but also on whether
locally more or less throughfall (δP_{TF}) was received and on local soil moisture conditions ($\delta\theta_{pre}$). In the subsoil additionally
macroporosity affected the soil moisture response directly. All main effects are also included in interactions, meaning that a
third variable influenced the relationship between an independent and dependent variable. For example, locally elevated
throughfall enhanced the soil water increase, but more so with increasing event size (Figure 5c,d, interaction $\hat{P}_{TF}$ x δP_{TF} ,
365   visualized in Figure 6a and 6b).

Spatial patterns of pre-event (or initial or drained) soil water content ($\delta\theta_{pre}$) notably affected top- and subsoil differently, making it the only factor yielding opposite effects on soil water content increase in different soil depths. In topsoil, drier locations stored less water per event than moister spots (positive slope estimates), whereas in subsoil, the opposite was the case (negative slope estimates). Notably, the slope of the interaction changes with overall soil water conditions consistently in both depths (Figure 5c and 5d, interaction $\hat{\theta}_{pre}$ x $\delta\theta_{pre}$, visualized in Figure 7): In very dry soil conditions (summer, topsoil), locally moister soil admitted more water into the soil (positive slope in Figure 7a), but less in overall wet conditions (negative slope in spring topsoil, permanently in subsoil). That influence of pre-event soil moisture patterns on moistening increased with event size (significant interaction $\hat{P}_{TF}$ x $\delta\theta_{pre}$, not visualized).
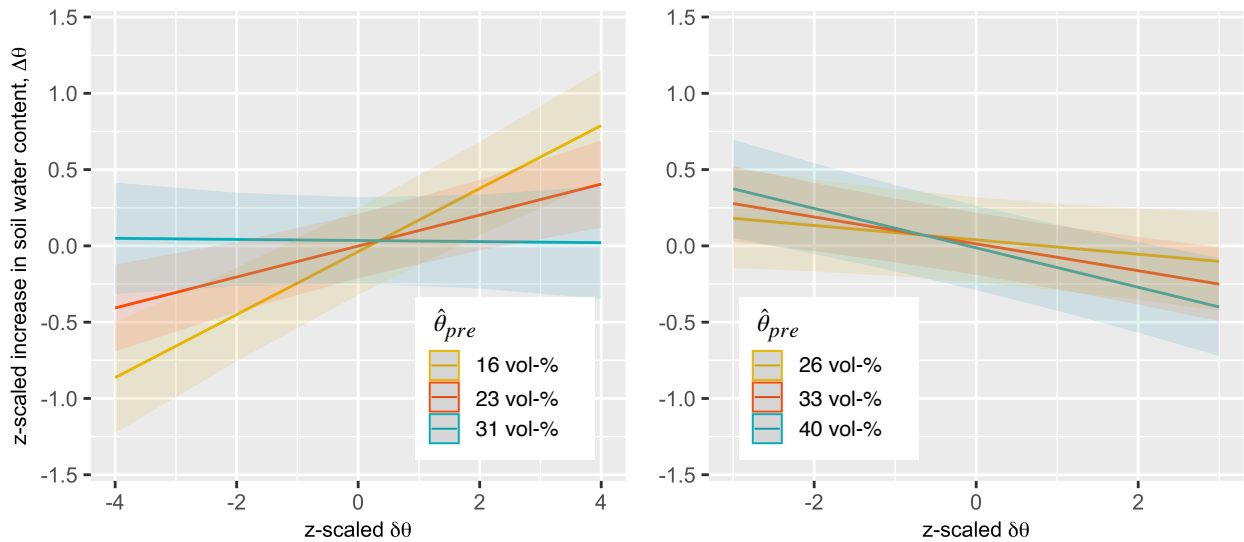
Fig 7. Marginal plot of the interaction between initial soil water content pattern (deviation of pre-event soil water content from the spatial median) and median soil water content ($\delta\theta_{pre}$ x $\hat{\theta}_{pre}$) affecting soil water content increase ($\Delta\theta$) for all events in topsoil (left) and subsoil (right). Groups indicate the overall soil moisture conditions (spatial median of pre-event soil water content, $\hat{\theta}_{pre}$), graphs show the relation between initial soil water pattern and local soil moisture response. All values are z-scaled, such that the slope indicates not only direction but also strength of the effect. For example, the blue line shows how in overall moist conditions (e.g. early spring), soil moisture response to rain is dampened in moister locations (high values of $\delta\theta_{pre}$) and more prominently so in the subsoil. Additionally, when topsoil soil is dry (e.g. summer, red, yellow line), also dry locations store less water. In combination, this leads to a change in slope direction in topsoil over the year. Subsoil water contents are always higher than those in topsoil, hence showing negative slopes (dampening in moist locations) throughout.

Additionally, in topsoil distance to the next tree affected the soil water response. Locations near trees reacted stronger to event precipitation than those further away (interactions $\hat{P}_{TF}$ x d_{tree}), but only in overall moister soil conditions (Figure 5c and 5d,

interaction $\hat{\theta}_{\mathrm{pre}}$ x d_{tree}). In the subsoil higher macroporosity (θ_{MP}), dampened the soil water response (Figure 5c and 5d, negative slope), and more so when or where throughfall was high (Figure 5c and 5d, interactions $\hat{P}_{TF}$ x θ_{MP} and θ_{MP} x δP_{TF}) as well as in drier locations (Figure 5c and 5d , interaction θ_{MP} x $\delta\theta_{\mathrm{pre}}$).

4 Discussion

4.1 Strengths and weaknesses of the approach

In this analysis we used extensive spatial data of canopy cover, throughfall and soil water content in order to assess the role of canopy processes on below-ground soil water response to precipitation. For this, we measured precipitation and soil water content at different locations in order to avoid disturbance of soil water dynamics by the precipitation measurement and providing independent random measurement designs. To be able to relate observations at different locations, we used geostatistical methods to predict throughfall values at locations where soil water content was measured. Throughfall spatial prediction was based on an extensive dataset of a substantial number (n=350) of samplers of comparatively small size (support is A=0.011 m^2) in a stratified random design, spanning an extent more than 10 times the correlation lengths of most events. Throughfall showed strong spatial autocorrelation which was reflected by 90% of the nugget-to-still ratios lower than 10% (Table S3). With the tight sampling at shortest lag distance (at least 50 locations covered two samplers located directly next to each other), the nugget effect, or unresolved variance, can be attributed to the dispersion variance across the sampler (support) and the spatial field shifting slightly within the rain event. Choice of support scale affects the variance estimate as demonstrated for throughfall by Zuecco et al. (2014). Here, the scale of the sampler and that of the soil moisture sensors are roughly the same and thus the variance is appropriately captured for the intended purpose. Spatial correlation depended on event size in that the correlation length decreased with increasing event rainfall (see examples in Fig S4). In larger events this decreased the range within which throughfall could be predicted, and increased the number of locations with high kriging variance that were removed from the analysis. As a result, this decreased the sample size for large compared to small and medium sized events. Regardless, for all sampled events, we could still rely on datasets of 59 points on average.

In order to estimate a reliable variogram, we had to remove spatial outliers contaminating the sample, which demonstrates that throughfall spatial field is not entirely smooth. Outlier locations comprised on average 2.2% of the spatial sample, were rarely recurring, and were not only, but for large events mainly, related to throughfall hotspots. Throughfall hotspots have been related to interrupted flowlines leading to dripping points (Crockford and Richardson, 2000; Herwitz, 1987; Nanko et al., 2022; Staelens et al., 2006; Zimmermann et al., 2009) that can also move around slightly (Keim et al., 2005). In removing those outliers, our analysis neglects the role of dripping points on soil moisture response. Additionally, kriging tends to smooth the estimates compared to the actual data (Oliver and Webster, 2014). However, here the predicted throughfall showed approximately the same median and spatial variance as the measured data (without outliers), indicating that this was not a concern and the real variation was captured after the prediction procedure. Unfortunately, there is no perfect way to relate measurements obtained at different locations to each other. However, the combination of a large sample size of throughfall, a

420 stratified design, outlier detection using robust variogram estimators and using residual maximum likelihood (REML) are established tools for estimating the variogram reliably (Lark, 2000; Voss et al., 2016). The latter provides an essential basis for kriging (Oliver and Webster, 2014). Cross-validation of the kriging estimates against observations (Lark, 2000; Oliver and Webster, 2014) provides further confidence in the variogram and kriging procedure for interpolating the aboveground data to the belowground locations.

425 In our analysis we quantified only throughfall input and omit the role of stemflow, which may play a role in locations near stems. Extrapolating stemflow input to soil moisture locations entails more prediction steps compared to throughfall. Spatial variation of stemflow depends on the one hand on species, tree and canopy size, neighborhood and individual morphology of the trees (Bellot and Escarre, 1998; Fan et al., 2015a; Levia et al., 2014; Levia and Germer, 2015; Magliano et al., 2019; Metzger et al., 2019; Van Stan et al., 2016) and on the other hand on precipitation intensity and soil conditions determining

430 the infiltration area (Carlyle-Moses et al., 2018; Herwitz, 1986; Metzger et al., 2021). Such a prediction would not only introduce a great deal of uncertainty, but also deviate from the main purpose of this study, which is to evaluate the role of throughfall heterogeneity. Therefore, in the model analysis, microsites near stems were accounted for by including distance to the stem as fixed effect in the model. This takes into account to some extent the potential influence of stemflow in the interpretation.

4.2 General patterns of throughfall (temporal and spatial)

In agreement with previous studies, spatial variation coefficients of throughfall decrease with event size (Aussenac, 1970; Carlyle-Moses, 2004; Llorens et al., 1997; Loustau et al., 1992; Metzger et al., 2017; Staelens et al., 2008; Su et al., 2019; Van Stan et al., 2020). Several other studies have suggested that the spatial variation of throughfall depends on the amount of precipitation as well as to canopy characteristics also (Carlyle-Moses, 2004; Herwitz and Slye, 1995; Hsueh et al., 2016; Keim

440 et al., 2005; Loustau et al., 1992; Park and Cameron, 2008; Zimmermann et al., 2009). Similarly, at our site for all event size classes, canopy cover was a significant driver of throughfall spatial distribution, although a small one compared to the random effects. Spatial trends showed no clear pattern with event size and may have been related to a combination of slope aspect and wind conditions. The correlation length (effective range) of throughfall decreased with increasing event size and corresponded for medium events roughly to that of canopy cover. The change of spatial pattern with event size underlines that not only

445 canopy storage per se, but also other processes like turbulence, wind shadows, the arrangement of canopy gaps, or the formation of canopy dripping points can add persistent spatial organization to below-canopy precipitation (Carlyle-Moses, 2004; Keim et al., 2005; Li et al., 2016; Park and Cameron, 2008; Staelens et al., 2008; Van Stan et al., 2020; Wullaert et al., 2009; Zimmermann et al., 2008). Additionally, canopy features also affect within canopy re-distribution (André et al., 2011; Herwitz, 1987; Levia and Frost, 2006; Nanko et al., 2022) which could lead to reoccurring patterns not reflected by canopy density.

450 Overall, and despite the slight changes in throughfall correlation lengths for different events size classes, throughfall patterns were temporally stable, indicating the existence of permanent hot and cold spots of throughfall, and those were consistent

across small, medium and large events. This is in line with several previous studies stating temporal stability of throughfall patterns (Fan et al., 2015a; Fathizadeh et al., 2014; Keim et al., 2005; Metzger et al., 2017; Molina et al., 2019; Rodrigues et al., 2022; Staelens et al., 2006; Wullaert et al., 2009; Zhu et al., 2021; Zimmermann et al., 2009) even over several years
455 (Rodrigues et al., 2022; Wullaert et al., 2009), although phenology and canopy development have also been observed to deteriorate spatial stability (Fathizadeh et al., 2014; Zimmermann et al., 2008). Furthermore, although spatial variation coefficients are smaller in large compared to small events, absolute values vary much more in large events such that they have arguably a higher potential to induce spatial patterns in soil water content or dynamics.

4.3 General soil water content patterns and potential drivers

460 Mean soil water contents were generally lower in the topsoil compared to the subsoil. At our site, the shallow soil is underlain by undulating weathered calcareous bedrock (Kohlhepp et al., 2017) of low hydraulic conductivity, and may locally be broken through by tree roots. While the topsoil is well-drained (i.e. saturated to field capacity in winter and much lower in summer), the deeper and finer textured soil layer (Metzger et al., 2021) is influenced by the much less conductive regolith and generally moister soil water content which very occasionally exceeds field capacity in winter (Metzger et al., 2017).

465 Much in agreement with previous studies in humid regions (Brocca et al., 2007; Korres et al., 2015; Metzger et al., 2017; Rosenbaum et al., 2012), spatial variation of soil water content increased in both top- and subsoil in drier summer soil conditions. In an earlier study at the same site a strong but short-lived increase of spatial variation of topsoil water content in summer was related to precipitation events (Metzger et al., 2017). Regardless, we found that the main controlling factor of post-event soil water content was the spatial pattern of pre-event soil water content, while average throughfall and spatial
470 pattern of throughfall, tree distance and macroporosity were additional, but much less important drivers. In other words, while soil water content variation increases strongly after events, this variation can only in very limited fashion be traced back to input patterns. This may in part be due to the small inputs of water compared to the overall soil water storage, leading to a strong memory effect of the pre-event soil water conditions on the post event patterns. Furthermore, preferential flow already taking place during the event itself can blur the throughfall pattern within the soil storage (see below).

475 Soil water content spatial patterns in drained state in turn were strongly driven by random effects. Those are factors that were not described by the measurements, but are temporally stable. Those so called local soil conditions are potentially related to soil hydraulic properties, root water uptake and microtopography (Famiglietti et al., 1998; Fan et al., 2015b; Vereecken et al., 2007). The mixed-effects models confirm, although with a very weak influence, that locations of higher macroporosity were drier in both depths, confirming the role of water retention on soil water patterns (Metzger et al., 2017) at this site. Also,
480 throughfall patterns of the previous event slightly affected topsoil pre-event soil water content. Thus, an imprint of the throughfall pattern was carried over to the next pre-event soil conditions, but this is barely detectable and negligible compared to the other sources of variation in soil water content in drained state.

4.4 Drivers of soil water response (Δθ) to rainfall

In contrast to the absolute values of soil water contents discussed above, the local soil water response (i.e. increase of soil water content following rainfall events), was clearly affected by the spatial throughfall pattern both in top- and subsoil, although modified by soil properties. Since we tested the effect of the spatial pattern (δP_{TF}) separately from the absolute values of event throughfall ($\hat{P}_{TF}$), we are able to demonstrate the influence of spatial throughfall fields specifically. Among all drivers tested, the influence of spatial throughfall variation was not necessarily the strongest, but consistently re-occurring factor. It appeared in both observed soil depths with similar influence, and was more pronounced for larger events. In other words, spatial variation of throughfall was a consistent driver of soil wetting.

Measurements ascertaining that soil water content response relates to canopy drainage patterns are comparatively rare. Metzger et al. (2017) previously reported for the same site, but a smaller dataset, that increases in soil water content were correlated with event spatial throughfall patterns during larger rainfall events. Molina et al. (2019), using highly temporally resolved soil moisture measurements, found a relationship between the average throughfall pattern and the soil water content response in the topsoil of a Mediterranean oak dominated forest plot, but not in a pine plot. Notably, Klos et al. (2014) showed in a tropical rainforest that locations of high and low soil water content below the main rooting zone corresponded to the end members of high and low throughfall, while soil water content above and below this depth was more homogenous. They concluded from additional modelling that preferential flow may have contributed to bypassing the main rooting zone. On the other hand, several studies, such as Raat et al. (2002), Shachnovich and Berliner, (2008), and more recently Zhu et al. (2021) using less temporally resolved soil water content measurements (incidentally all in coniferous forests) found no relationships between the spatial patterns of soil water content and throughfall. All authors report that the throughfall patterns were pronounced and stable in time and suggest that the forests floor impeded the transfer to soil water patterns. An additional explanation could be that the effect of spatial net precipitation patterns on soil water content was so short-lived due to preferential flow (Metzger et al., 2017) that it was not observed by infrequent hand measurements. Overall, the stronger soil water response at sites with above average throughfall indicates that throughfall hot spots and also cold spots (Levia and Frost, 2006; Van Stan et al., 2020; Zimmermann et al., 2009) have an impact on soil water dynamics, although they go almost unnoticed in the soil water content pattern (see above).

In addition to the throughfall pattern, the soil water response after large rainfall events also depended on the pattern of pre-event soil water content at both depths. Notably, the slope of the relationship changes direction, making it the only factor that shows opposite effects in the top- and subsoil. This can be attributed to its inter-dependence on soil water content, and the difference in moisture between the two measurement depths. Especially under dry (summer) conditions, wetter topsoil locations stored more of the incoming precipitation water, while drier sites remained dry. This is a strong indication of preferential flow in dry soils, where, for example, hydrophobic conditions, cracks and low hydraulic conductivity of the matrix can enhance preferential flow (Beven and Germann, 2013; Hillel, 1998; Nimmo, 2021). On the other hand, the dampened water response in the wetter subsoil, could be due to enhanced hydraulic conductivity and less free pore space (Hagen et al.,

2020; Vereecken et al., 2007). It is noteworthy that effects in dry conditions are much stronger than in wet conditions, suggesting a stronger trigger for preferential flow there. Moreover, only in intermediate soil water contents the spatial distribution of soil water contents had no influence on the spatial drainage behavior.

Soil water response depended additionally also on the distance to the nearest tree in the topsoil and soil properties (macroporosity) in the subsoil. The enhanced moistening of soils near stems is likely related to stemflow production (Metzger et al., 2019), which was not accounted for as input. Stemflow production generally increases with event size (Levia and Germer, 2015; Metzger et al., 2019), explaining the interaction in the model. The additional modification by soil water conditions can be explained by the systematically lower soil water contents near tree trunks at the same site (Metzger et al., 2021, 2017), due to lower soil water retention and likely enhanced drainage there.

Taken together, our data strongly suggest that additionally to spatial distribution of throughfall, the spatial pattern in drainage behaviour affects the local soil water response to rainfall. In that, both dry and wet locations can, water supply permitting, act as percolation hotspots, depending on the overall soil conditions. Bypass flow in forests has been repeatedly observed (Bachmair et al., 2012; Blume et al., 2009; Demand et al., 2019; e.g. Schume et al., 2003; Schwärzel et al., 2009) especially in dry summer conditions (Bachmair et al., 2012; Demand et al., 2019; Schume et al., 2003). Spatial variation of infiltration water supply and intensity, such as is the case for below canopy precipitation (Keim and Link, 2018), has been suggested as a potential cause for initiating finger flow (Nimmo, 2021), which is promoted by dry soil conditions. Also, hydrophobicity has been suggested to contribute to maintaining recurring finger flow paths (Blume et al., 2009). Furthermore, macropore flow along biopores (Lange et al., 2009; Nespoulous et al., 2019) and soil cracks (Schume et al., 2003) can be enhanced in dry forest soil conditions due to soil shrinking (Baram et al., 2012). While both finger flow and macropore flow may have contributed to the observed patterns in soil water response, macropore flow more than finger flow could explain enhanced matter export (Lehmann et al., 2021) as well as fast response following strong storms observed in the shallow aquifers of the AquaDiva Critical Zone Observatory (Lehmann and Totsche, 2020).

Overall, our results confirm that the effect of throughfall on soil water content is weak, but stronger on the soil water response. This contrasts with previous modelling (Coenders-Gerrits et al., 2013) that did not account for preferential flow. As the effect of the throughfall pattern on the soil water response also depends on local conditions related to hydraulic properties, its fate is much more likely to be found in the drainage fluxes, rather than the soil water storage. The further destiny of the net precipitation pattern arguably depends on the deeper subsurface hydrogeological setting. We deduce however, that net precipitation hotspots have a strong chance of producing patterns of preferential flow below the main rooting zone, which is in line with previous work (Klos et al., 2014), and backs earlier hypotheses (Bouten et al., 1992; Schume et al., 2003).

5 Conclusion

In this study, we collected an extensive dataset to investigate the effect of throughfall spatial heterogeneity on the soil water response and checked which other factors (pre-event soil water content, macroporosity, tree distance) modified the result.

We first confirmed that throughfall patterns were stable in time and found that they related to the vegetation canopy density, although additional and partly unknown factors strongly affected throughfall distribution. We found that post event soil

550 water content per se did have a very weak relation to throughfall, although the variation of soil water content clearly increased in the aftermath of rain events. The post-event soil water content pattern was overwhelmingly determined by the strong memory effect of the soil water storage and only slightly affected by soil properties, like macroporosity. In contrast, the soil water response showed a clear relation with the throughfall input pattern. In other words, our setup allowed us to confirm experimentally that throughfall patterns do imprint on soil water content dynamics, at least shortly after rain events.

555 However, we also identified locations where soil water response was dampened, likely due to enhanced fast drainage. Those locations could be either very dry locations likely promoting preferential flow, especially in the topsoil, or wet locations, promoting faster release of the incoming water. Our results demonstrate that throughfall spatial patterns leave a stronger imprint on soil water dynamics than on soil water content directly, and explain why aboveground influence on soil hydrology has been so difficult to lay open in the past. Our results are in line with previous research and contribute a more

560 general process understanding of the below ground consequences of precipitation redistribution by forests. Most importantly, our results strongly suggest that throughfall patterns induce fast soil water flow with repeating spatial patterns. Those patterns would therefore already be triggered within the canopy.

Acknowledgements

565 We thank Murray Lark for insightful comments on the strategy for comparing above and belowground spatial patterns that helped shaping the geostatistical analysis. We thank Beate and Alexander Zimmermann for sharing their insights, workflow and routines for variogram prediction with us. We also thank two anonymous reviewers for insightful and constructive feedback that improved this manuscript.

This study is part of the Collaborative Research Centre AquaDiva of the Friedrich Schiller University Jena, funded by the

570 Deutsche Forschungsgemeinschaft (DFG, German Research Foundation) – SFB 1076 – Project Number 218627073. We thank the Hainich CZE site manager Robert Lehmann and the Hainich National Park. Field work permits were issued by the responsible state environmental offices of Thüringen.

Data availability

575 The dataset is currently prepared for publishing in a official repository. The doi will be posted with the data at the latest when the data is published.

Author contributions

AH developed the project idea. All authors contributed to the collection of the raw data. CF conducted the statistical analysis, developed it further with AH, and both wrote the first draft of the manuscript. All authors contributed to discussion and writing of the manuscript.

References

André, F., Jonard, M., Jonard, F., Ponette, Q., 2011. Spatial and temporal patterns of throughfall volume in a deciduous mixed-species stand. Journal of Hydrology 400, 244–254. https://doi.org/10.1016/j.jhydrol.2011.01.037

Aussenac, G., 1970. Action du couvert forestier sur la distribution au sol des précipitations. Annales des Sciences Forestières 27, 383–399. https://doi.org/10.1051/forest/19700403

Bachmair, S., Weiler, M., Troch, P.A., 2012. Intercomparing hillslope hydrological dynamics: Spatio-temporal variability and vegetation cover effects. Water Resources Research 48, 1–18. https://doi.org/10.1029/2011WR011196

Baram, S., Kurtzman, D., Dahan, O., 2012. Water percolation through a clayey vadose zone. Journal of Hydrology 424–425, 165–171. https://doi.org/10.1016/j.jhydrol.2011.12.040

Barton, K., 2020. MuMIn: Multi-Model Inference.

Bates, D., Mächler, M., Bolker, B., Walker, S., 2015. Fitting Linear Mixed-Effects Models Using lme4. Journal of Statistical Software 67, 1–48. https://doi.org/10.18637/jss.v067.i01

Bellot, J., Escarre, A., 1998. Stemflow and throughfall determination in a resprouted Mediterranean holm-oak forest. Annales des Sciences Forestières 55, 847–865. https://doi.org/10.1051/forest:19980708

Beven, K., Germann, P., 2013. Macropores and water flow in soils revisited. Water Resources Research accepted. https://doi.org/10.1002/wrcr.20156

Blume, T., Zehe, E., Bronstert, a., 2009. Use of soil moisture dynamics and patterns at different spatio-temporal scales for the investigation of subsurface flow processes. Hydrology and Earth System Sciences 13, 1215–1233. https://doi.org/10.5194/hess-13-1215-2009

Bogena, H.R., Herbst, M., Huisman, J.A., Rosenbaum, U., Weuthen, A., Vereecken, H., 2010. Potential of Wireless Sensor Networks for Measuring Soil Water Content Variability. Vadoze Zone Journal 9, 1002–1013. https://doi.org/10.2136/vzj2009.0173

Bouten, W., Heimovaara, T.J., Tiktak, A., 1992. Spatial patterns of throughfall and soil water dynamics in a Douglas fir stand. Water Resources Research 28, 3227–3233. https://doi.org/10.1029/92WR01764

Brocca, L., Morbidelli, R., Melone, F., Moramarco, T., 2007. Soil moisture spatial variability in experimental areas of central Italy. Journal of Hydrology 333, 356–373. https://doi.org/10.1016/j.jhydrol.2006.09.004

Brown, A.E., Zhang, L., McMahon, T.A., Western, A.W., Vertessy, R.A., 2005. A review of paired catchment studies for determining changes in water yield resulting from alterations in vegetation. Journal of Hydrology 310, 28–61.

https://doi.org/10.1016/j.jhydrol.2004.12.010

Carlyle-Moses, D.E., 2004. Throughfall, stemflow, and canopy interception loss fluxes in a semi-arid Sierra Madre Oriental matorral community. Journal of Arid Environments 58, 181–202. https://doi.org/10.1016/S0140-1963(03)00125-3

Carlyle-Moses, D.E., Gash, J.H.C., 2011. Rainfall Interception Loss by Forest Canopies, in: Levia, D.F., Carlyle-Moses, D.E., Tanaka, T. (Eds.), Forest Hydrology and Biogeochemistry: Synthesis of Past Research and Future Directions, Ecological Studies 216. Spinger Science+Buisness Media, pp. 407–423. https://doi.org/10.1007/978-94-007-1363-5

Carlyle-Moses, D.E., Iida, S., Germer, S., Llorens, P., Michalzik, B., Nanko, K., Tischer, A., Levia, D.F., 2018. Expressing stemflow commensurate with its ecohydrological importance. Advances in Water Resources 121, 472–479. https://doi.org/10.1016/j.advwatres.2018.08.015

Coenders-Gerrits, A.M.J., Hopp, L., Savenije, H.H.G., Pfister, L., 2013. The effect of spatial throughfall patterns on soil moisture patterns at the hillslope scale. Hydrology and Earth System Sciences 17, 1749–1763. https://doi.org/10.5194/hess-17-1749-2013

Cressie, N., Hawkins, D.M., 1980. Robust estimation of the variogram: I. Mathematical Geology 12, 115–125. https://doi.org/10.1007/BF01035243

Crockford, R.H., Richardson, D.P., 2000. Partitioning of rainfall into throughfall, stemflow and interception: effect of forest type, ground cover and climate. Hydrological Processes 14, 2903–2920. https://doi.org/10.1002/1099-1085(200011/12)14:16/17<2903::AID-HYP126>3.0.CO;2-6

Demand, D., Blume, T., Weiler, M., 2019. Spatio-temporal relevance and controls of preferential flow at the landscape scale. Hydrology and Earth System Sciences 23, 4869–4889. https://doi.org/10.5194/hess-23-4869-2019

Dowd, P.A., 1984. The Variogram and Kriging: Robust and Resistant Estimators, in: Verly, G., David, M., Journel, A.G., Marechal, A. (Eds.), Geostatistics for Natural Resources Characterization: Part 1. Springer Netherlands, Dordrecht, pp. 91–106. https://doi.org/10.1007/978-94-009-3699-7_6

Durocher, M.G., 1990. Monitoring spatial variability of forest interception. Hydrological Processes 4, 215–229.

Falkengren-Grerup, U., 1989. Effect of stemflow on beech forest soils and vegetation in southern Sweden. Plant Ecology 26, 341–352.

Famiglietti, J.S., Rudnicki, J.W., Rodell, M., 1998. Variability in surface moisture content along a hillslope transect: Rattlesnake Hill, Texas. Journal of Hydrology 210, 259–281. https://doi.org/10.1016/S0022-1694(98)00187-5

Fan, J., Oestergaard, K.T., Guyot, A., Jensen, D.G., Lockington, D.A., 2015a. Spatial variability of throughfall and stemflow in an exotic pine plantation of subtropical coastal Australia. Hydrological Processes 29, 793–804. https://doi.org/10.1002/hyp.10193

Fan, J., Scheuermann, A., Guyot, A., Baumgartl, T., Lockington, D.A., 2015b. Quantifying spatiotemporal dynamics of root-zone soil water in a mixed forest on subtropical coastal sand dune using surface ERT and spatial TDR. Journal of Hydrology 523, 475–488. https://doi.org/10.1016/j.jhydrol.2015.01.064

Fathizadeh, O., Attarod, P., Keim, R.F., Stein, A., Amiri, G.Z., Darvishsefat, A.A., 2014. Spatial heterogeneity and temporal

stability of throughfall under individual Quercus brantii trees. Hydrological Processes 28, 1124–1136. https://doi.org/10.1002/hyp.9638

Genton, M.G., 1998. Highly Robust Variogram Estimation. Mathematical Geology 30, 213–221. https://doi.org/10.1023/A:1021728614555

Germer, S., 2013. Development of near-surface perched water tables during natural and artificial stemflow generation by babassu palms. Journal of Hydrology 507, 262–272. https://doi.org/10.1016/j.jhydrol.2013.10.026

Gerrits, A.M.J., Savenije, H.H.G., 2011. Forest Floor Interception, in: Levia, D.F., Carlyle-Moses, D., Tanaka, T. (Eds.), Forest Hydrology and Biogeochemistry: Synthesis of Past Research and Future Directions. Springer Netherlands, Dordrecht, pp. 445–454. https://doi.org/10.1007/978-94-007-1363-5_22

Gräler, B., Pebesma, E., Heuvelink, G., 2016. Spatio-Temporal Interpolation using gstat. The R Journal 8, 204–218.

Guswa, A.J., 2012. Canopy vs. Roots: Production and Destruction of Variability in Soil Moisture and Hydrologic Fluxes. Vadose Zone Journal 11. https://doi.org/10.2136/vzj2011.0159

Guswa, A.J., Spence, C.M., 2012. Effect of throughfall variability on recharge: Application to hemlock and deciduous forests in western Massachusetts. Ecohydrology 5, 563–574. https://doi.org/10.1002/eco.281

Guswa, A.J., Tetzlaff, D., Selker, J.S., Carlyle-Moses, D.E., Boyer, E.W., Bruen, M., Cayuela, C., Creed, I.F., van de Giesen, N., Grasso, D., Hannah, D.M., Hudson, J.E., Hudson, S.A., Iida, S., Jackson, R.B., Katul, G.G., Kumagai, T., Llorens, P., Lopes Ribeiro, F., Michalzik, B., Nanko, K., Oster, C., Pataki, D.E., Peters, C.A., Rinaldo, A., Sanchez Carretero, D., Trifunovic, B., Zalewski, M., Haagsma, M., Levia, D.F., 2020. Advancing ecohydrology in the 21st century: A convergence of opportunities. Ecohydrology 13, 1–14. https://doi.org/10.1002/eco.2208

Hagen, K., Berger, A., Gartner, K., Geitner, C., Kofler, T., Kogelbauer, I., Kohl, B., Markart, G., Meißl, G., Niedertscheider, K., 2020. Event-based dynamics of the soil water content at Alpine sites (Tyrol, Austria). Catena 194. https://doi.org/10.1016/j.catena.2020.104682

Herwitz, S.R., 1987. Raindrop impact and water flow on the vegetative surfaces of trees and the effects on stemflow and throughfall generation. Earth Surf. Process. Landforms 12, 425–432. https://doi.org/10.1002/esp.3290120408

Herwitz, S.R., 1986. Infiltration-excess caused by Stemflow in a cyclone-prone tropical rainforest. Earth Surf. Process. Landforms 11, 401–412. https://doi.org/10.1002/esp.3290110406

Herwitz, S.R., Slye, R.E., 1995. Three-dimensional modeling of canopy tree interception of wind-driven rainfall. Journal of Hydrology 168, 205–226. https://doi.org/10.1016/0022-1694(94)02643-P

Hillel, D., 1998. Environmental Soil Physics. Academic Press, Boston.

Horton, R.E., 1919. Rainfall Interception. Monthly Weather Review 47, 603–623. https://doi.org/10.1175/1520-0493(1919)47<603:RI>2.0.CO;2

Hsueh, Y.H., Allen, S.T., Keim, R.F., 2016. Fine-scale spatial variability of throughfall amount and isotopic composition under a hardwood forest canopy. Hydrological Processes 30, 1796–1803. https://doi.org/10.1002/hyp.10772

Keim, R., Skaugset, a, Weiler, M., 2005. Temporal persistence of spatial patterns in throughfall. Journal of Hydrology 314,

263–274. https://doi.org/10.1016/j.jhydrol.2005.03.021

680   Keim, R.F., Link, T.E., 2018. Linked spatial variability of throughfall amount and intensity during rainfall in a coniferous forest. Agricultural and Forest Meteorology 248, 15–21. https://doi.org/10.1016/j.agrformet.2017.09.006

Kimmins, J.P., 1973. Some Statistical Aspects of Sampling Throughfall Precipitation in Nutrient Cycling Studies in British Columbian Coastal Forests. Ecology 54, 1008–1019. https://doi.org/10.2307/1935567

Klos, P.Z., Chain-Guadarrama, A., Link, T.E., Finegan, B., Vierling, L.A., Chazdon, R., 2014. Throughfall heterogeneity in
685   tropical forested landscapes as a focal mechanism for deep percolation. Journal of Hydrology 519, 2180–2188. https://doi.org/10.1016/j.jhydrol.2014.10.004

Kohlhepp, B., Lehmann, R., Seeber, P., Küsel, K., Trumbore, S.E., Totsche, K.U., 2017. Aquifer configuration and geostructural links control the groundwater quality in thin-bedded carbonate-siliciclastic alternations of the Hainich CZE, central Germany. Hydrology and Earth System Sciences 21, 6091–6116. https://doi.org/10.5194/hess-21-6091-2017

690   Korres, W., Reichenau, T.G., Fiener, P., Koyama, C.N., Bogena, H.R., Cornelissen, T., Baatz, R., Herbst, M., Diekkrüger, B., Vereecken, H., Schneider, K., 2015. Spatio-temporal soil moisture patterns – A meta-analysis using plot to catchment scale data. Journal of Hydrology 520, 326–341. https://doi.org/10.1016/j.jhydrol.2014.11.042

Küsel, K., Totsche, K.U., Trumbore, S.E., Lehmann, R., Steinhäuser, C., Herrmann, M., 2016. How Deep Can Surface Signals Be Traced in the Critical Zone? Merging Biodiversity with Biogeochemistry Research in a Central German Muschelkalk
695   Landscape. Frontiers in Earth Science 4, 1–18. https://doi.org/10.3389/feart.2016.00032

Kuznetsova, A., Brockhoff, P.B., Christensen, R.H.B., 2017. lmerTest Package: Tests in Linear Mixed Effects Models. Journal of Statistical Software 82, 1–26. https://doi.org/10.18637/jss.v082.i13

Lange, B., Lüescher, P., Germann, P.F., 2009. Significance of tree roots for preferential infiltration in stagnic soils. Hydrology and Earth System Sciences 13, 1809–1821. https://doi.org/10.5194/hess-13-1809-2009

700   Lark, R.M., 2000. A comparison of some robust estimators of the variogram for use in soil survey. European Journal of Soil Science 51, 137–157. https://doi.org/10.1046/j.1365-2389.2000.00280.x

Lehmann, K., Lehmann, R., Totsche, K.U., 2021. Event-driven dynamics of the total mobile inventory in undisturbed soil account for significant fluxes of particulate organic carbon. Science of the Total Environment 756, 143774. https://doi.org/10.1016/j.scitotenv.2020.143774

705   Lehmann, R., Totsche, K.U., 2020. Multi-directional flow dynamics shape groundwater quality in sloping bedrock strata. Journal of Hydrology 580, 124291. https://doi.org/10.1016/j.jhydrol.2019.124291

Levia, D.F., Frost, E.E., 2006. Variability of throughfall volume and solute inputs in wooded ecosystems. Progress in Physical Geography: Earth and Environment 30, 605–632. https://doi.org/10.1177/0309133306071145

Levia, D.F., Germer, S., 2015. A review of stemflow generation dynamics and stemflow-environment interactions in forests
710   and shrublands. Reviews of Geophysics 53, 673–714. https://doi.org/10.1002/2015RG000479.Received

Levia, D.F., Michalzik, B., Näthe, K., Bischoff, S., Richter, S., Legates, D.R., 2014. Differential stemflow yield from European beech saplings: The role of individual canopy structure metrics. Hydrological Processes. https://doi.org/10.1002/hyp.10124

Li, X., Xiao, Q., Niu, J., Dymond, S., van Doorn, N.S., Yu, X., Xie, B., Lv, X., Zhang, K., Li, J., 2016. Process-based rainfall interception by small trees in Northern China: The effect of rainfall traits and crown structure characteristics. Agricultural and Forest Meteorology 218–219, 65–73. https://doi.org/10.1016/j.agrformet.2015.11.017

Liang, W.-L., Kosugi, K., Mizuyama, T., 2007. Heterogeneous Soil Water Dynamics around a Tree Growing on a Steep Hillslope. Vadose Zone Journal 6, 879–889. https://doi.org/10.2136/vzj2007.0029

Liang, W.L., Li, S.L., Hung, F.X., 2017. Analysis of the contributions of topographic, soil, and vegetation features on the spatial distributions of surface soil moisture in a steep natural forested headwater catchment. Hydrological Processes 31, 3796–3809. https://doi.org/10.1002/hyp.11290

Llorens, P., Poch, R., Latron, J., Gallart, F., 1997. Rainfall interception by a Pinus sylvestris forest patch overgrown in a Mediterranean mountainous abandoned area I. Monitoring design and results down to the event scale. Journal of Hydrology 199, 331–345. https://doi.org/10.1016/S0022-1694(96)03334-3

Lloyd, C.R., Marques, A.D.O., 1988. Spatial variability of throughfall and stemflow measurements in Amazonian rainforest. Agricultural and Forest Meteorology 42, 63–73. https://doi.org/10.1016/0168-1923(88)90067-6

Loustau, D., Berbigier, P., Granier, A., 1992. Interception loss, throughfall and stemflow in a maritime pine stand. II. An application of Gash's analytical model of interception. Journal of Hydrology 138, 469–485. https://doi.org/10.1016/0022-1694(92)90131-E

Magliano, P.N., Whitworth-Hulse, J.I., Florio, E.L., Aguirre, E.C., Blanco, L.J., 2019. Interception loss, throughfall and stemflow by *Larrea divaricata* : The role of rainfall characteristics and plant morphological attributes. Ecological Research 34, 753–764. https://doi.org/10.1111/1440-1703.12036

Matheron, G., 1962. Traité de géostatistique appliquée, Mémoires du Bureau de Recherches Géologiques et Minières. Éditions Technip, Paris.

Metzger, J.C., Filipzik, J., Michalzik, B., Hildebrandt, A., 2021. Stemflow Infiltration Hotspots Create Soil Microsites Near Tree Stems in an Unmanaged Mixed Beech Forest. Frontiers in Forests and Global Change 4, 1–14. https://doi.org/10.3389/ffgc.2021.701293

Metzger, J.C., Schumacher, J., Lange, M., Hildebrandt, A., 2019. Neighbourhood and stand structure affect stemflow generation in a heterogeneous deciduous temperate forest. Hydrology and Earth System Sciences 23. https://doi.org/10.5194/hess-23-4433-2019

Metzger, J.C., Wutzler, T., Dalla Valle, N., Filipzik, J., Grauer, C., Lehmann, R., Roggenbuck, M., Schelhorn, D., Weckmüller, J., Küsel, K., Totsche, K.U., Trumbore, S., Hildebrandt, A., 2017. Vegetation impacts soil water content patterns by shaping canopy water fluxes and soil properties. Hydrological Processes 31, 3783–3795. https://doi.org/10.1002/hyp.11274

Molina, A.J., Llorens, P., Garcia-Estringana, P., Moreno de las Heras, M., Cayuela, C., Gallart, F., Latron, J., 2019. Contributions of throughfall, forest and soil characteristics to near-surface soil water-content variability at the plot scale in a mountainous Mediterranean area. Science of The Total Environment 647, 1421–1432. https://doi.org/10.1016/j.scitotenv.2018.08.020

Murray, S.J., 2014. Trends in 20th century global rainfall interception as simulated by a dynamic global vegetation model: Implications for global water resources. Ecohydrology 7, 102–114. https://doi.org/10.1002/eco.1325

Nakagawa, S., Schielzeth, H., 2013. A general and simple method for obtaining R^2 from generalized linear mixed-effects models. Methods Ecol Evol 4, 133–142. https://doi.org/10.1111/j.2041-210x.2012.00261.x

Nanko, K., Keim, R.F., Hudson, S.A., Levia, D.F., 2022. Throughfall drop sizes suggest canopy flowpaths vary by phenophase. Journal of Hydrology 612, 128144. https://doi.org/10.1016/j.jhydrol.2022.128144

Nespoulous, J., Merino-Martín, L., Monnier, Y., Bouchet, D.C., Ramel, M., Dombey, R., Viennois, G., Mao, Z., Zhang, J.-L., Cao, K.-F., Le Bissonnais, Y., Sidle, R.C., Stokes, A., 2019. Tropical forest structure and understorey determine subsurface flow through biopores formed by plant roots. CATENA 181, 104061. https://doi.org/10.1016/j.catena.2019.05.007

Nimmo, J.R., 2021. The processes of preferential flow in the unsaturated zone. Soil Science Society of America Journal 85, 1–27. https://doi.org/10.1002/saj2.20143

Oda, T., Egusa, T., Ohte, N., Hotta, N., Tanaka, N., Green, M.B., Suzuki, M., 2021. Effects of changes in canopy interception on stream runoff response and recovery following clear-cutting of a Japanese coniferous forest in Fukuroyamasawa Experimental Watershed in Japan. Hydrological Processes 35, 1–14. https://doi.org/10.1002/hyp.14177

Oliver, M.A., Webster, R., 2014. A tutorial guide to geostatistics: Computing and modelling variograms and kriging. Catena 113, 56–69. https://doi.org/10.1016/j.catena.2013.09.006

Papritz, A., Schwierz, C., 2020. Package 'georob.'

Park, A., Cameron, J.L., 2008. The influence of canopy traits on throughfall and stemflow in five tropical trees growing in a Panamanian plantation. Forest Ecology and Management 255, 1915–1925. https://doi.org/10.1016/j.foreco.2007.12.025

Pebesma, E.J., 2004. Multivariable geostatistics in S: the gstat package. Computers & Geosciences 30, 683–691. https://doi.org/10.1016/j.cageo.2004.03.012

Pressland, A.J., 1976. Soil Moisture Redistribution as Affected by Throughfall and Stemflow in an Arid Zone Shrub Community. Australian Journal of Botany 24, 641–649.

Raat, K.J., Draaijers, G.P.J., Schaap, M.G., Tietema, A., Verstraten, J.M., 2002. Spatial variability of throughfall water and chemistry and forest floor water content in a Douglas fir forest stand. Hydrology and Earth System Sciences 6, 363–374. https://doi.org/10.5194/hess-6-363-2002

Ribeiro Jr, P.J., Diggle, P.J., 2001. geoR: A Package for Geostatistical Analysis. R-NEWS 1, 15–18.

Rodrigues, A.F., Terra, M.C.N.S., Mantovani, V.A., Cordeiro, N.G., Ribeiro, J.P.C., Guo, L., Nehren, U., Mello, J.M., Mello, C.R., 2022. Throughfall spatial variability in a neotropical forest: Have we correctly accounted for time stability? Journal of Hydrology 608. https://doi.org/10.1016/j.jhydrol.2022.127632

Rosenbaum, U., Bogena, H.R., Herbst, M., Huisman, J.A., Peterson, T.J., Weuthen, A., Western, A.W., Vereecken, H., 2012. Seasonal and event dynamics of spatial soil moisture patterns at the small catchment scale. Water Resources Research 48, W10544. https://doi.org/10.1029/2011WR011518

Savenije, H.H.G., 2004. The importance of interception and why we should delete the term evapotranspiration from our

vocabulary. Hydrological Processes 18, 1507–1511. https://doi.org/10.1002/hyp.5563

Schrumpf, M., Kaiser, K., Schulze, E.-D., 2014. Soil Organic Carbon and Total Nitrogen Gains in an Old Growth Deciduous Forest in Germany. PLoS ONE 9, e89364. https://doi.org/10.1371/journal.pone.0089364

Schume, H., Jost, G., Katzensteiner, K., 2003. Spatio-temporal analysis of the soil water content in a mixed Norway spruce (Picea abies (L.) Karst.)-European beech (Fagus sylvatica L.) stand. Geoderma 112, 273–287. https://doi.org/10.1016/S0016-7061(02)00311-7

Schwärzel, K., Menzer, A., Clausnitzer, F., Spank, U., Häntzschel, J., Grünwald, T., Köstner, B., Bernhofer, C., Feger, K.H., 2009. Soil water content measurements deliver reliable estimates of water fluxes: A comparative study in a beech and a spruce stand in the Tharandt forest (Saxony, Germany). Agricultural and Forest Meteorology 149, 1994–2006. https://doi.org/10.1016/j.agrformet.2009.07.006

Shachnovich, Y., Berliner, P.R., Bar, P., 2008. Rainfall interception and spatial distribution of throughfall in a pine forest planted in an arid zone. Journal of Hydrology 349, 168–177. https://doi.org/10.1016/j.jhydrol.2007.10.051

Staelens, J., De Schrijver, A., Verheyen, K., Verhoest, N.E.C., 2008. Rainfall partitioning into throughfall, stemflow, and interception within a single beech (Fagus sylvatica L.) canopy: influence of foliation, rain event characteristics, and meteorology. Hydrological Processes 22, 33–45. https://doi.org/10.1002/hyp

Staelens, J., De Schrijver, A., Verheyen, K., Verhoest, N.E.C., 2006. Spatial variability and temporal stability of throughfall water under a dominant beech (Fagus sylvatica L.) tree in relationship to canopy cover. Journal of Hydrology 330, 651–662. https://doi.org/10.1016/j.jhydrol.2006.04.032

Su, L., Xie, Z., Xu, W., Zhao, C., 2019. Variability of throughfall quantity in a mixed evergreen-deciduous broadleaved forest in central China. Journal of Hydrology and Hydromechanics 67, 225–231. https://doi.org/10.2478/johh-2019-0008

Vachaud, G., Passerat De Silans, A., Balabanis, P., Vauclin, M., 1985. Temporal Stability of Spatially Measured Soil Water Probability Density Function. Soil Science Society of America Journal 49, 822–828. https://doi.org/10.2136/sssaj1985.03615995004900040006x

Van Stan, J.T., Hildebrandt, A., Friesen, J., Metzger, J.C., Yankine, S.A., 2020. Spatial Variability and Temporal Stability of Local Net Precipitation Patterns, in: Van Stan, II, J.T., Gutmann, E., Friesen, J. (Eds.), Precipitation Partitioning by Vegetation. Springer International Publishing, Cham, pp. 89–104. https://doi.org/10.1007/978-3-030-29702-2_6

Van Stan, J.T., Lewis, E.S., Hildebrandt, A., Rebmann, C., Friesen, J., 2016. Impact of interacting bark structure and rainfall conditions on stemflow variability in a temperate beech-oak forest, central Germany. Hydrological Sciences Journal 61, 2071–2083. https://doi.org/10.1080/02626667.2015.1083104

Vereecken, H., Kamai, T., Harter, T., Kasteel, R., Hopmans, J., Vanderborght, J., 2007. Explaining soil moisture variability as a function of mean soil moisture: A stochastic unsaturated flow perspective. Geophysical Research Letters 34, 1–6. https://doi.org/10.1029/2007GL031813

Voss, S., Zimmermann, B., Zimmermann, A., 2016. Detecting spatial structures in throughfall data: The effect of extent, sample size, sampling design, and variogram estimation method. Journal of Hydrology 540, 527–537.

815   https://doi.org/10.1016/j.jhydrol.2016.06.042

Western, A.W., Zhou, S.L., Grayson, R.B., McMahon, T.A., Blöschl, G., Wilson, D.J., 2004. Spatial correlation of soil moisture in small catchments and its relationship to dominant spatial hydrological processes. Journal of Hydrology 286, 113–134. https://doi.org/10.1016/j.jhydrol.2003.09.014

Wullaert, H., Pohlert, T., Boy, J., Valarezo, C., Wilcke, W., 2009. Spatial throughfall heterogeneity in a montane rain forest

820   in   Ecuador: Extent,   temporal   stability   and   drivers.   Journal   of   Hydrology   377,   71–79. https://doi.org/10.1016/j.jhydrol.2009.08.001

Zehe, E., Graeff, T., Morgner, M., Bauer, a., Bronstert, a., 2010. Plot and field scale soil moisture dynamics and subsurface wetness control on runoff generation in a headwater in the Ore Mountains. Hydrology and Earth System Sciences 14, 873–889. https://doi.org/10.5194/hess-14-873-2010

825   Zhu, X., He, Z., Du, J., Chen, L., Lin, P., Tian, Q., 2021. Spatial heterogeneity of throughfall and its contributions to the variability in near-surface soil water-content in semiarid mountains of China. Forest Ecology and Management 488. https://doi.org/10.1016/j.foreco.2021.119008

Zimmermann, A., Germer, S., Neill, C., Krusche, A.V., Elsenbeer, H., 2008. Spatio-temporal patterns of throughfall and solute deposition in an open tropical rain forest. Journal of Hydrology 360, 87–102. https://doi.org/10.1016/j.jhydrol.2008.07.028

830   Zimmermann, A., Voss, S., Metzger, J.C., Hildebrandt, A., Zimmermann, B., 2016. Capturing heterogeneity: The role of a study   area's   extent   for   estimating   mean   throughfall.   Journal   of   Hydrology   542,   781–789. https://doi.org/10.1016/j.jhydrol.2016.09.047

Zimmermann, A., Zimmermann, B., 2014. Requirements for throughfall monitoring: The roles of temporal scale and canopy complexity. Agricultural and Forest Meteorology 189–190, 125–139. https://doi.org/10.1016/j.agrformet.2014.01.014

835   Zimmermann, A., Zimmermann, B., Elsenbeer, H., 2009. Rainfall redistribution in a tropical forest: Spatial and temporal patterns. Water Resources Research 45, 1–18. https://doi.org/10.1029/2008WR007470

Zimmermann, B., Zimmermann, A., Lark, R.M., Elsenbeer, H., 2010. Sampling procedures for throughfall monitoring: A simulation study. Water Resources Research 46, 1–15. https://doi.org/10.1029/2009WR007776

Zuecco, G., Penna, D., van Meerveld, H.J., Hopp, L., Fontana, G.D., Borga, M., 2014. Comparison of two different types of

840   throughfall collectors.